Composites Part B 191 (2020) 107961

Contents lists available at ScienceDirect

Composites Part B

journal homepage: www.elsevier.com/locate/compositesb

# Fabrication of eco-friendly and multifunctional sodium-containing polyhedral oligomeric silsesquioxane and its flame retardancy on epoxy resin

Xinming Ye [a,b], Jingjing Li [a], Wenchao Zhang [a], Rongjie Yang [a,*], Jiarong Li [b]

[a] National Engineering Technology Research Center of Flame Retardant Material, School of Materials, Beijing Institute of Technology, 5 South Zhongguancun Street, Haidian District, Beijing, 100081, PR China

[b] School of Chemistry and Chemical Engineering, Beijing Institute of Technology, 5 South Zhongguancun Street, Haidian District, Beijing, 100081, PR China

ARTICLE INFO

*Keywords:*
Epoxy resin
Na-Ph-POSS
Flame retardancy
Smoke suppression
Dielectric constant

ABSTRACT

Considering the reduction of fire hazards associated with the application of epoxy resin (EP) composites. Herein, a novel sodium-containing polyhedral oligomeric phenyl silsesquioxane (Na-Ph-POSS) has been synthesized through hydrolysis condensation. FTIR, NMR and MALDI-TOF MS results reveal that Na-Ph-POSS is a hepta-phenyl POSS consisting of Si–O–Na and Si–OH groups. Compared to pure EP, according to the combustion results, the peak of heat release rate (p-HRR), the maximum smoke density (Ds, max) and the peak of CO production rate (p-COP) of EP/5 wt% Na-Ph-POSS significantly decrease by 45.9, 45.1 and 46.9%, respectively. Additionally, EP composites endowed with Na-Ph-POSS have low dielectric constant and dielectric loss. Therefore, eco-friendly multifunctional Na-Ph-POSS provides a promising prospect for mitigating the fire hazards of EP composites.

## 1. Introduction

Polymeric materials are widely used in our lives due to their outstanding corrosion resistance, lightweight and easy processing. However, most of them are extremely flammable, and release a lot of smoke and toxic volatiles during the combustion process [1,2]. For instance, the practical applications of epoxy resin (EP) are seriously restricted by its high combustibility [3–5]. In order to overcome the shortcoming, flame retardants are introduced into EP to enhance the flame retardancy [6–11].

Incorporation of halogen-based flame retardants into polymer matrix can achieve pleasurable flame retardancy. Nonetheless, the halogen-containing compounds generate corrosive toxic volatiles during combustion, and these toxic gaseous products cause serious environmental problems. Therefore, halogen-based flame retardants are forbidden [12,13]. Metal oxides and metal hydroxides are used as halogen-free effective flame retardants to improve the flame retardancy of polymers. However, they often require a large amount of addition to achieve the desired flame retardant effect [14,15]. This drawback inevitably deteriorates the comprehensive performance of composites.

Recent developments in the field of composites have led to a renewed interest in flame retardants. Halogen-free nano-scale flame retardants are increasingly promising due to their excellent flame retardancy at intensely low loading levels [16–18]. Polyhedral oligomeric silsesquioxane (POSS) is considered to be an overwhelmingly effective 0-dimensional non-toxic, halogen-free and environmentally friendly organic-inorganic nanohybrid flame retardant [19,20]. Trisilanol hepta-phenyl polyhedral oligomeric silsesquioxane ($T_7$-Ph-POSS) and phosphorus-containing POSS (Table S1) were synthesized by our group [21,22]. However, incorporating $T_7$-Ph-POSS (Table S1) into EP alone did not show favorable flame retardant effects. When combined with an aluminum-containing catalyst, the dispersed particle size of $T_7$-Ph-POSS in EP was reduced, which in turn the combustion properties were enhanced [23].

In addition, some specific metal elements have excellent catalytic carbonization performances during combustion [24]. For instance, copper phenylphosphate (CuPP) nanoplates were synthesized by Wang et al. [25], and incorporating 4 wt% CuPP into EP could significantly increase the value of LOI and decrease the release of heat and toxic volatiles. Zinc ferrite (ZF) was adopted to decorate boron nitride nanosheet (BNNS) prepared by Zhang et al., which demonstrated that ZF nanofiller acted as the catalyst to enhance catalytic charring of EP

* Corresponding author.
*E-mail address:* yrj@bit.edu.cn (R. Yang).

https://doi.org/10.1016/j.compositesb.2020.107961
Received 13 January 2020; Received in revised form 29 February 2020; Accepted 4 March 2020
Available online 8 March 2020

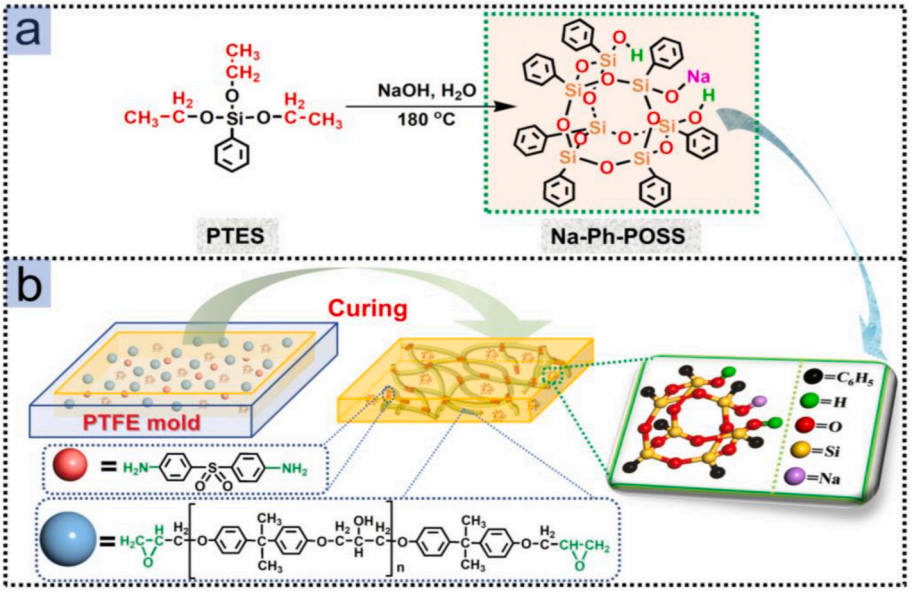


**Fig. 1.** Synthesis route (a) of Na-Ph-POSS and schematic illustration of curing process (b) for EP/Na-Ph-POSS.

composites. Thereby the toxic volatiles were significantly suppressed by the compact char layers [26]. Carbon nanotubes (CNTs) wrapped with $MoS_2$ nanolayers ($MoS_2$-CNTs) were synthesized by Hu et al. [27], and the evolution of toxic CO and other gaseous products during EP composites decomposition were dramatically decreased after incorporating $MoS_2$-CNTs. Therefore, if some certain metal elements can be grafted into the POSS nanocage by chemical synthesis methods, metal elements containing POSS will be obtained [28,29]. Titanium-containing POSS (Table S1) was synthesized and used in EP, both char yield and LOI value of the modified EP composites were increased significantly at a loading range of 1.5–6.0 wt% [30]. However, due to the expensive materials and complicate synthesis of metallic POSS (M-POSS), few studies have been conducted to introduce M-POSS into polymer materials as flame retardants.

From the perspectives of environmental protection, fire safety and simplified synthesis process, in this work, an incompletely condensed sodium-containing phenyl polyhedral oligomeric silsesquioxane (Na-Ph-POSS) (Table S1) has been successfully prepared via one-pot method. Then, $T_7$-Ph-POSS or Na-Ph-POSS was introduced into EP with the same amount, and the effects of trace Na in the POSS nanocage on the flame retardancy of EP composite were discussed in detail. Finally, the synergistic mechanism of flame retardant and smoke suppression related to

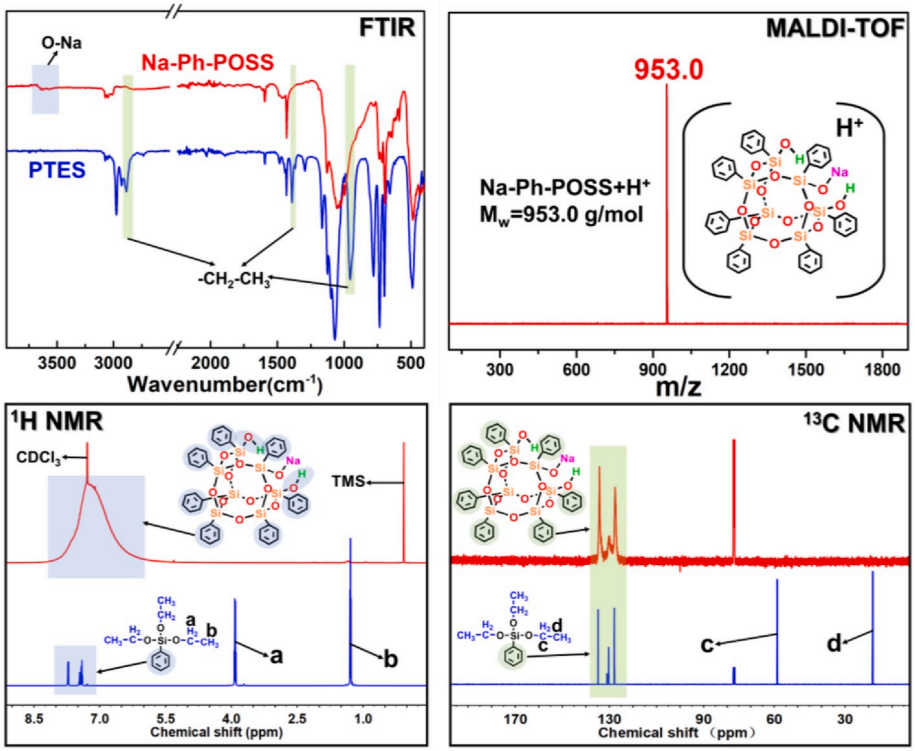


**Fig. 2.** FTIR, MALDI-TOF MS, $^1$H and $^{13}$C NMR spectra of Na-Ph-POSS and PTES.

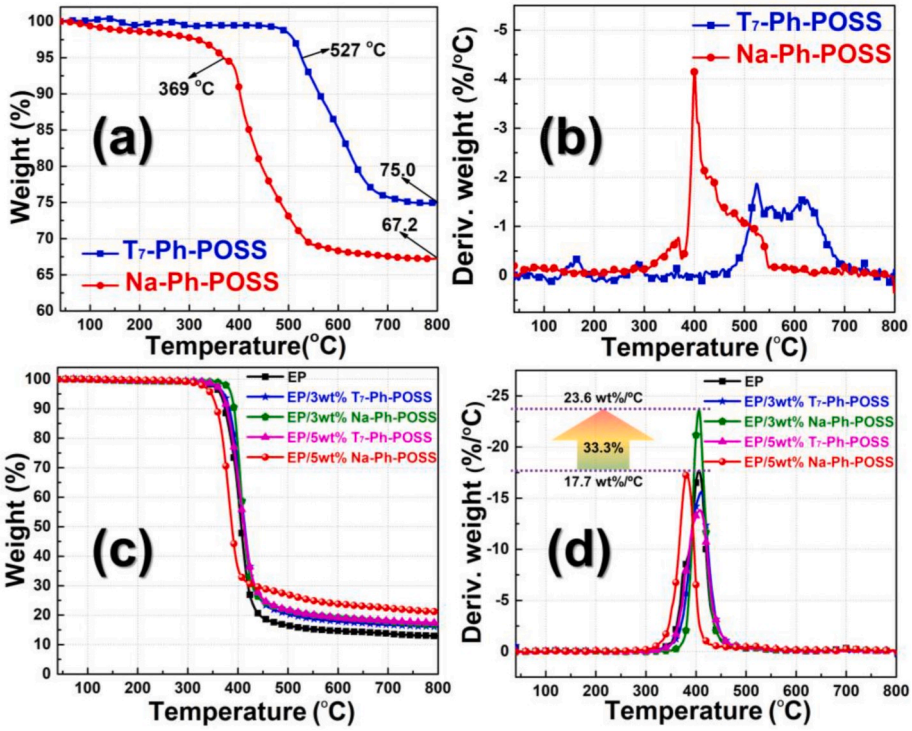


**Fig. 3.** TGA (a, c) and DTG (b, d) curves of $T_7$-Ph-POSS, Na-Ph-POSS, EP, EP/$T_7$-Ph-POSS and EP/Na-Ph-POSS under $N_2$ atmosphere.

Na and Si was proposed for the first time.

## 2. Experimental section

### 2.1. Materials

NaOH and acetone were obtained from Beijing Chemical Works. Phenyltriethoxysilane (PTES, >99%) was purchased from JiangHan Fine Chemical. Diglycidyl ether of bisphenol A (DGEBA, E44) was supplied by FeiCheng DeYuan Chemicals Co., Ltd. 4,4-diaminodiphenylsulphone (DDS, >98.0%) was purchased from Tianjin Guangfu Fine Chemical Research Institute. $T_7$-Ph-POSS was synthesized by our laboratory. All solvents and reagents were used as received without any further purification.

### 2.2. Synthesis of the Na-Ph-POSS

The synthetic route of Na-Ph-POSS is illustrated in Fig. 1 (a). First, NaOH (2.8 g, 0.4 mol), $H_2O$ (3.36 mL), PTES (31.32 g, 0.13 mol), and acetone (100 mL) were mixed in a dry 250 mL three-necked flask equipped with magnetic stirring. Then the mixture was heated to reflux and stirred for 16–20 h. The resulting mixture was filtered to give an insoluble white solid power, and the white solid product was washed several times with acetone. Na-Ph-POSS was obtained after drying for 6–8 h in a blast oven at 180 °C.

### 2.3. Fabrication of EP and its composite with POSS

The $T_7$-Ph-POSS or Na-Ph-POSS was introduced into DGEBA (E44), and stirring for 60–90 min to dissolve sufficiently at 140 °C. Then, DDS was incorporated into the liquid mixture and stirred for 30 min. Finally, the resulting mixture was rapidly poured into a polytetrafluoroethylene (PTFE) mold and cured at 180 °C for 4 h. A similar preparation procedure for EP (DGEBA-DDS). The curing process of EP/Na-Ph-POSS is presented in Fig. 1 (b), and the contents in EP composites are displayed in Table S2.

### 2.4. Characterizations

The characterizations adopted in this article are listed in the **Electronic Supplementary Information**.

## 3. Results and discussion

### 3.1. Chemical structural characterization

As illustrated in FTIR spectra (Fig. 2). In comparison with PTES, the Na-Ph-POSS exhibited several same characteristic peaks at 1120 $cm^{-1}$ (Ph-Si), 1429 and 1593 $cm^{-1}$ (C═C in benzene ring units). In addition, there were several absorption peaks appeared at 980-1100 $cm^{-1}$ in Na-Ph-POSS spectra, which attributed to Si–O–Si and Si–O [31,32]. Moreover, a small wide peak at 3660 $cm^{-1}$ was caused by the absorbance of the O–Na group. Furthermore, the characteristic absorption peaks of 959, 1391, and 2888 $cm^{-1}$ were assigned to the $–CH_2$-$CH_3$ in PTES completely disappeared in Na-Ph-POSS, which implied that the hydrolysis polycondensation reaction of PTES was complete.

As for the $^1$H NMR spectra (Fig. 2), similar to the FTIR spectra results, the characteristic signals of $–CH_2$-$CH_3$ (a and b) were disappeared in the $^1$H NMR spectra of Na-Ph-POSS, which further proved that PTES was completely hydrolyzed. Particularly, an obvious broad peak appeared at 6.0–8.0 ppm for the $^1$H NMR spectra of Na-Ph-POSS, which was assigned to the hydrogen proton signals in phenyls and Si–OH groups. Furthermore, as illustrated in the $^{13}$C NMR spectra (Fig. 2), the characteristic signals at 58.7 ppm (c) and 18.1 ppm (d) were corresponded to $–CH_2$ and $–CH_3$ in PTES disappeared completely, meanwhile, the typical signals of phenyl groups at 125–140 ppm still remained. FTIR and NMR results demonstrated that PTES underwent complete hydrolysis action in the presence of NaOH and $H_2O$ to generate a product containing Si–OH and Si–O–Na groups.

The MALDI-TOF MS spectra of Na-Ph-POSS was displayed in Fig. 2, only a signal peak at 953.0 [Na-Ph-POSS + $H^+$] could be observed, it was very close to the theoretical calculation value of 952 ($m/z$) (Na-Ph-POSS). This result meant that the synthesized product had a single

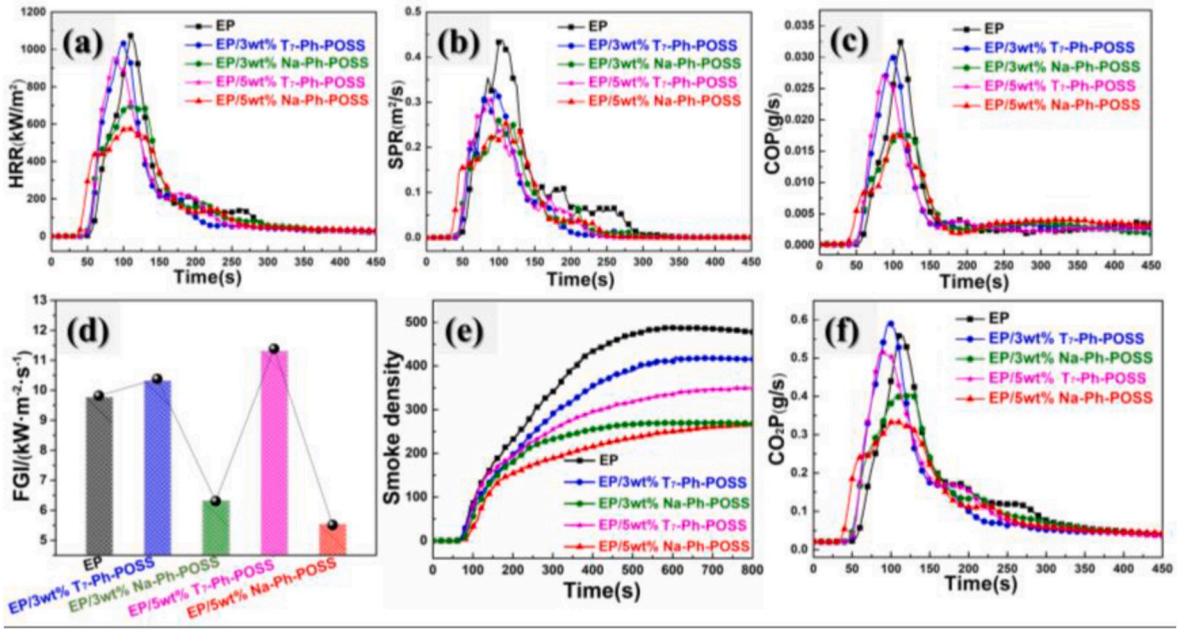


**Fig. 4.** HRR curves (a), SPR curves (b), COP curves (c), FGI data (d), smoke density curves (e) and $CO_2P$ curves (f) of EP and its composites.

structure and no other by-products were produced. Furthermore, as illustrated in Fig. S1, the atomic concentration of Na is 1.91%, which matched well with the theoretical calculation of 1.61% for Na-Ph-POSS. All the above results confirmed the Na-Ph-POSS was successfully prepared and it was an incomplete polycondensation cage structure endowed with Si–O–Na and Si–OH groups.

### 3.2. Thermal stability

As observed in Fig. 3 and Table S3, the degradation paths of $T_7$-Ph-POSS and Na-Ph-POSS were completely different, the initial degradation temperature (defined as the weight loss is 5%) of $T_7$-Ph-POSS and Na-Ph-POSS under nitrogen atmosphere were 527 and 369 °C, respectively. Moreover, the char residues of $T_7$-Ph-POSS and Na-Ph-POSS were 75.0 and 67.2 wt% at 800 °C, respectively. Therefore, $T_7$-Ph-POSS was endowed with better thermal stability. As listed in Table S4, the char residues of EP, EP/3 wt% $T_7$-Ph-POSS and EP/5 wt% $T_7$-Ph-POSS were 12.9, 16.1 and 17.4 wt% at 800 °C, respectively. It was obvious that when the addition amount of $T_7$-Ph-POSS was increased from 3 to 5 wt %, the char residues were increased slightly. In contrast, when the addition amount of Na-Ph-POSS was 3 wt%, the degradation of the EP/3 wt% Na-Ph-POSS was dramatically accelerated in the range of 360–450 °C. Upon increasing the incorporation amount of Na-Ph-POSS to 5 wt%, the residual char at 800 °C was sharply improved.

### 3.3. Fire hazards of EP and its composites

Diffusion of heat and toxic smoke is the main factor that cause significant harm to human life in a fire accident [33,34]. Herein, the cone calorimeter and smoke density tester were adopted to investigate the fire hazards of EP and its composites. Meanwhile, the cone calorimeter test can give some crucial relevant parameters, such as the time to ignition (TTI), peak of heat release rate (p-HRR), fire growth index (FGI), smoke production rate (SPR), CO production rate (COP) and $CO_2$ production rate ($CO_2P$) [35].

Generally, the heat generated in a real fire accident is one of the greatest threats to life and property safety. Therefore, p-HRR is a crucial indicator for evaluating the flame-retardant properties of polymeric materials. Fig. 4 exhibited the HRR curves (a) and FGI data (d) of EP and its composites. The value of p-HRR for EP, EP/5 wt% $T_7$-Ph-POSS and EP/5 wt% Na-Ph-POSS were 1074, 960 and 581 kW/m$^2$, respectively. Obviously, compared with $T_7$-Ph-POSS, the introduction of Na-Ph-POSS was more conducive to reducing the p-HRR of the modified EP composites. Meanwhile, there was another important indicator named "fire growth index (FGI)" that could be calculated from the ratio of p-HRR and the time to p-HRR ($t_{p\text{-}HRR}$), revealing the fire hazards of materials. The lower value of FGI meant lower fire hazards [26]. It was evident that incorporating $T_7$-Ph-POSS into EP made the value of FGI increase, in contrast, with the introduction of Na-Ph-POSS from 3 to 5 wt%, FGI values were remarkably decreased from 9.76 kW m$^{-2}$ s$^{-1}$ (pure EP) to 6.31 and 5.53 kW m$^{-2}$ s$^{-1}$, respectively. These results suggested that the incorporation of Na-Ph-POSS could apparently reduce the heat release and mitigate the danger of EP composites.

Cone calorimeter (Fig. 4b) and NBS smoke density tester (Fig. 4e) were adopted to detect the smoke produced during combustion. As displayed in Fig. 4b and listed in Table 1, introducing $T_7$-Ph-POSS or Na-Ph-POSS into EP could decrease the peak of smoke production rate (p-SPR). Compared to EP, the p-SPR of EP/3 wt% $T_7$-Ph-POSS and EP/5 wt % $T_7$-Ph-POSS were slightly reduced by 25.0 and 29.5%. However, the p-SPR of EP/3 wt% Na-Ph-POSS and EP/5 wt% Na-Ph-POSS were distinctly decreased by 40.9 and 43.2%. Similarly, just as shown in Fig. 4e, with increasing the incorporation of $T_7$-Ph-POSS from 3 to 5 wt

**Table 1**
Cone calorimeter data of EP and its composites.

| Samples | TTI (s) | p-HRR (kW/m$^2$) | $t_{p\text{-}HRR}$ (s) | FGI kW/(m$^2$·s) | p-SPR (m$^2$/s) | Ds, max | p-COP (g/s) | p-$CO_2$P (g/s) |
|---|---|---|---|---|---|---|---|---|
| EP | 36 ± 2 | 1074 ± 25 | 110 ± 1 | 9.76 ± 0.12 | 0.44 ± 0.08 | 488 ± 5 | 0.032 ± 0.006 | 0.56 ± 0.06 |
| EP/3 wt% $T_7$-Ph-POSS | 36 ± 1 | 1031 ± 22 | 100 ± 2 | 10.13 ± 0.11 | 0.33 ± 0.06 | 421 ± 8 | 0.030 ± 0.004 | 0.59 ± 0.03 |
| EP/3 wt% Na-Ph-POSS | 34 ± 3 | 694 ± 19 | 110 ± 3 | 6.31 ± 0.15 | 0.26 ± 0.03 | 270 ± 6 | 0.018 ± 0.005 | 0.41 ± 0.05 |
| EP/5 wt% $T_7$-Ph-POSS | 36 ± 2 | 960 ± 33 | 85 ± 2 | 11.30 ± 0.13 | 0.31 ± 0.05 | 350 ± 9 | 0.027 ± 0.007 | 0.51 ± 0.08 |
| EP/5 wt% Na-Ph-POSS | 29 ± 1 | 581 ± 21 | 105 ± 1 | 5.53 ± 0.11 | 0.25 ± 0.02 | 268 ± 3 | 0.017 ± 0.002 | 0.33 ± 0.02 |

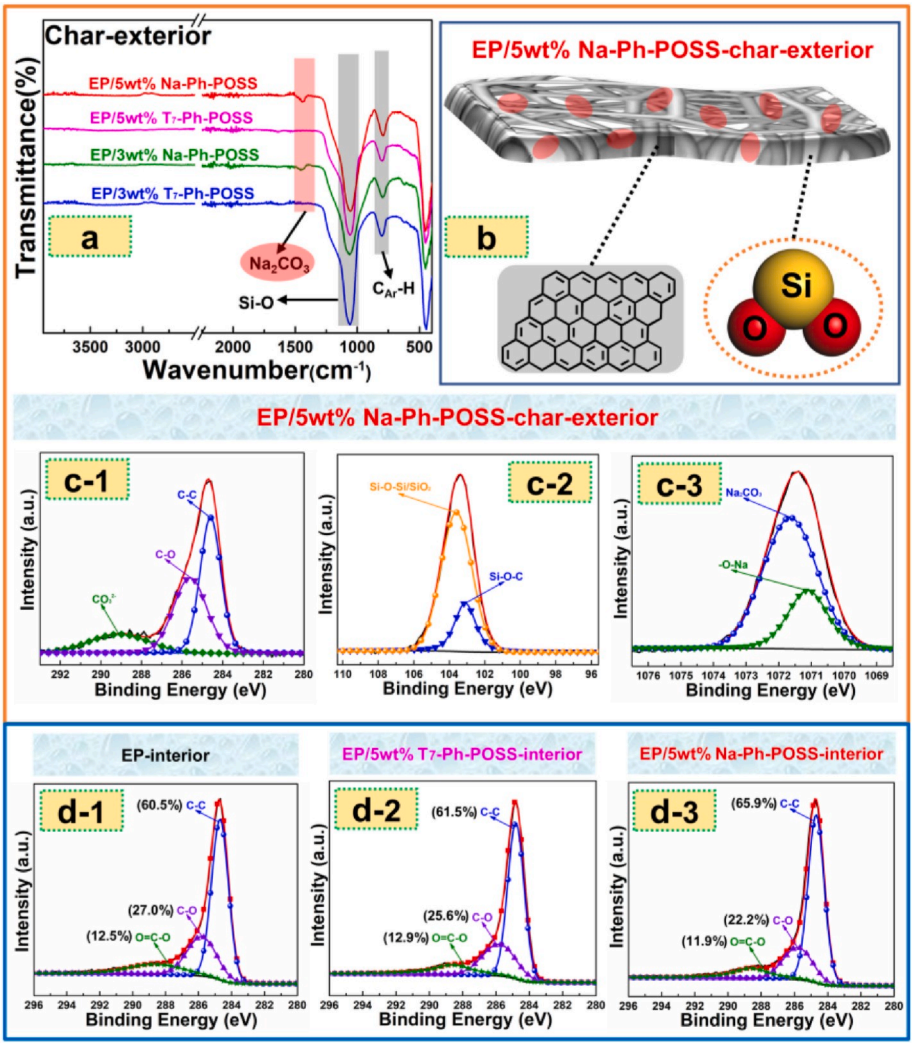


**Fig. 5.** FTIR spectra (a) of exterior char of EP composites; the schematic diagram (b) and high-resolution $C_{1s}$ (c-1), $Si_{2p}$ (c-2) and $Na_{1s}$ (c-3) XPS spectra of exterior char residues of EP/5 wt% Na-Ph-POSS; the high-resolution $C_{1s}$ XPS spectra of interior char residues for EP (d-1), EP/5 wt% $T_7$-Ph-POSS (d-2) and EP/5 wt% Na-Ph-POSS (d-3).

%, the reductions of the maximum smoke density (Ds, max) were 13.7 and 28.3%, respectively. Nonetheless, with increasing the addition of Na-Ph-POSS from 3 to 5 wt%, the values of the maximum smoke density were lower, and the reductions were 44.7 and 45.1%, respectively. Therefore, the smoke suppression effect of Na-Ph-POSS was more distinguished than $T_7$-Ph-POSS. These results further proved that Na-Ph-POSS could significantly decline the fire risk of EP composites.

CO (Fig. 4c) and $CO_2$ (Fig. 4f) production rate during the cone calorimeter test were chosen to investigate the generation of small molecular volatiles during combustion. Compared with $T_7$-Ph-POSS, the addition of Na-Ph-POSS into EP decreased the peak of CO production rate (p-COP) to a larger extent. The p-$CO_2$P for EP/3 wt% Na-Ph-POSS and EP/5 wt% Na-Ph-POSS dropped from 0.56 g/s to 0.41 g/s and 0.33 g/s, respectively.

**Table 2**
The high-resolution $C_{1s}$ XPS of interior char residues for EP, EP/5 wt% $T_7$-Ph-POSS and EP/5 wt% Na-Ph-POSS.

| Samples | C–C area (%) | C–O area (%) | O–C=O area (%) | $C_{ox}/C_a$ |
|---|---|---|---|---|
| EP | 60.5 | 27.0 | 12.5 | 0.65 |
| EP/5 wt% $T_7$-Ph-POSS | 61.5 | 25.6 | 12.9 | 0.63 |
| EP/5 wt% Na-Ph-POSS | 65.9 | 22.2 | 11.9 | 0.52 |

### 3.4. Catalytic charring mechanism

In order to further investigate the reason that Na-Ph-POSS could significantly inhibit the release of heat and smoke. The char residues of EP and its composites after cone calorimeter test were chosen, and the digital photographs were displayed in Fig. S2. Meanwhile, FTIR and XPS were employed to analyze the chemical structure of char layers obtained from cone calorimeter tests. As observed in Fig. 5a, the characteristic peak of Si–O was appeared at 1060 $cm^{-1}$. Therefore, the main component of the gray matter for exterior char layer was $SiO_2$. In particular, a absorption peak at 1457 $cm^{-1}$ could be assigned to $Na_2CO_3$, which might bridge the generated $SiO_2$ of the exterior char of EP/Na-Ph-POSS.

The high-resolution $C_{1s}$ (Figs. 5c–1), $Si_{2p}$ (Figs. 5c–2) and $Na_{1s}$ (Figs. 5c–3) XPS spectra of exterior char residues of EP/5 wt% Na-Ph-POSS could been recorded in Fig. 5. Peaks at 289.2, 285.8, and 284.6 eV were assigned to $CO_3^{2-}$, C–O and C–C/C–H [36,37], respectively. Meanwhile, the two peaks at 103.4 and 103.1 eV could be observed in $Si_{2p}$ spectra, they were correspnded to Si–O–Si and Si–O–C [38]. Similarly, the two peaks at 1071.8 and 1071.1 eV appeared in the $Na_{1s}$ spectra, they were attributed to $Na_2CO_3$ and -O-Na. These results further

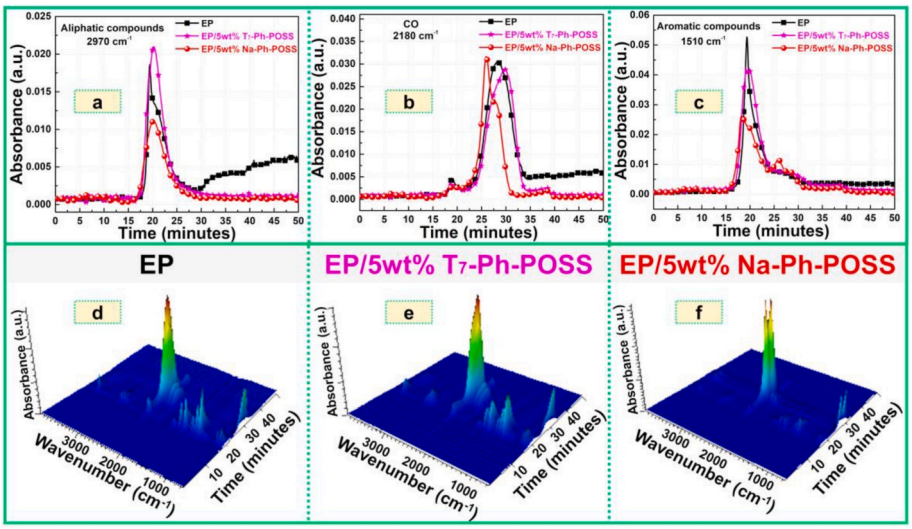


**Fig. 6.** The absorbance of aliphatic compounds (a), CO (b) and aromatic compounds (c) produced during the pyrolysis process and 3D TG-FTIR spectra of pyrolysis gaseous products for pure EP (d), EP/5 wt% $T_7$-Ph-POSS (e) and EP/5 wt% Na-Ph-POSS (f).

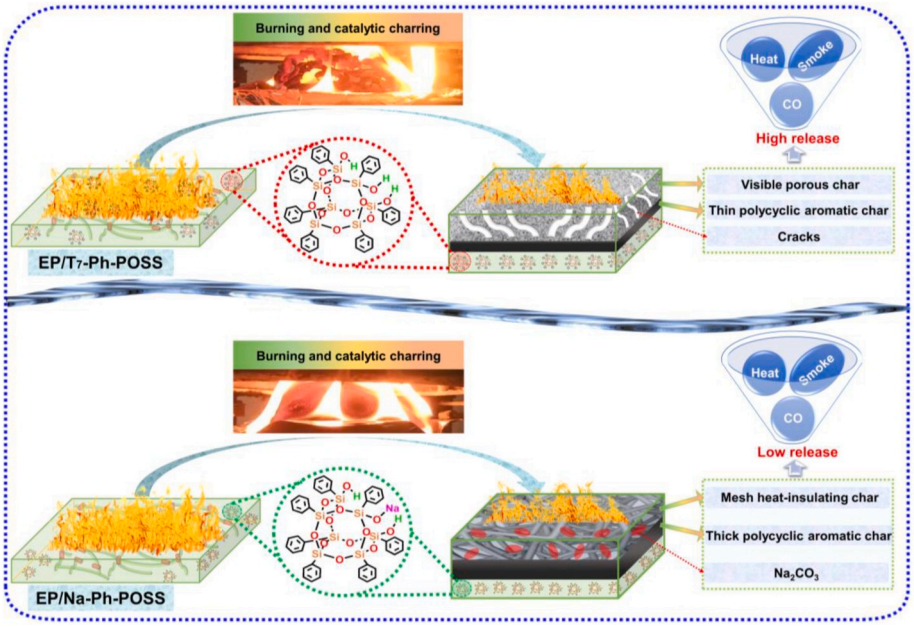


**Fig. 7.** Catalytic charring schematic illustration and digital photos during cone calorimeter test for EP/$T_7$-Ph-POSS and EP/Na-Ph-POSS.

proved the exterior char residues of EP/5 wt% Na-Ph-POSS was mainly consist of Si–O–Si, $Na_2CO_3$ and polycyclic aromatic compounds, and the schematic diagram was displayed in Fig. 5b.

The interior char residues of EP (Figs. 5d–1), EP/5 wt% $T_7$-Ph-POSS (Figs. 5d–2) and EP/5 wt% Na-Ph-POSS (Figs. 5d–3) were also characterized by XPS, and the corresponding data was listed in Table 2. Compared with EP, after adding $T_7$-Ph-POSS, the percentage of C–C bond area in the interior organic residual char was basically similar. On the contrary, after introducing Na-Ph-POSS, the percentage of C–C bond area was raised. Meanwhile, the $C_{ox}/C_a$ ($C_{ox}$ represents the content of the carbon atoms of C–O and O═C–O, $C_a$ represents the content of the carbon atoms of C–C and C–H) value of EP/5 wt% Na-Ph-POSS was the lowest, and the lower value of $C_{ox}/C_a$ meant the higher thermal oxidation resistance of the formed char layer [39]. Therefore, incorporating Na-Ph-POSS into EP could effectively enhance the thermal oxidation resistance of the interior char layer.

To futher explain the reasons for the smoke suppression effect of Na-Ph-POSS, the absorbance of aliphatic compounds (a), CO (b) and aromatic compounds (c) produced during the pyrolysis process and 3D TG-FTIR spectra of pyrolysis gaseous products for pure EP (d), EP/5 wt% $T_7$-Ph-POSS (e) and EP/5 wt% Na-Ph-POSS (f) were shown in Fig. 6. In comparison with EP, the addition of $T_7$-Ph-POSS could slightly reduce the absorption intensity of aromatic compounds and CO. Introducing Na-Ph-POSS into EP, the absorption intensity of aliphatic and aromatic compounds was distinctly decreased. In addition, after the addition of Na-Ph-POSS, although the production of CO was advanced in the second decomposed stage, the end time was notably earlier than EP and EP/5 wt % $T_7$-Ph-POSS. Therefore, the integral area of CO release was sharply lower than that of EP and EP/5 wt% $T_7$-Ph-POSS. This result was consistent with the results of the cone calorimeter test. All of the above analysis indicated that the introduction of Na-Ph-POSS could change the degradation path of EP composites, thereby inhibiting the release of these harmful and combustible gases.

According to the above analysis, the possible catalytic charring

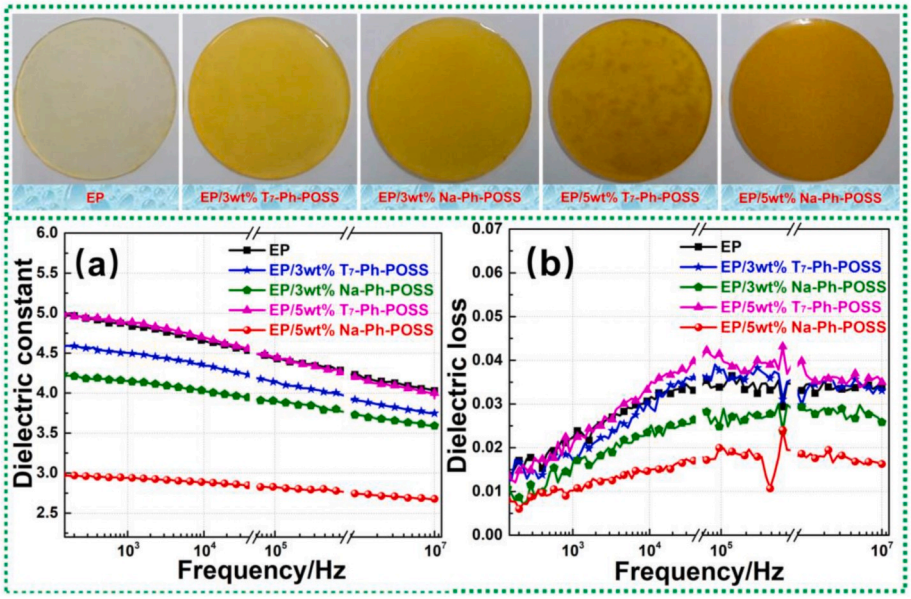


**Fig. 8.** Digital photos, the dielectric constant curves (a) and dielectric loss curves (b) of EP and its composites.

mechanism and digital photos during the cone calorimeter tests for EP/$T_7$-Ph-POSS and EP/Na-Ph-POSS are illustrated in Fig. 7. For EP/$T_7$-Ph-POSS, EP matrix of the heated surface is basically degraded or burned out, but the $T_7$-Ph-POSS inside does not undergo significant degradation. Therefore, obvious visible porous char layers are formed, which are extremely detrimental for protecting the substrate material from further combustion. In contrast, for EP/Na-Ph-POSS, the heated surface of EP/Na-Ph-POSS rapidly forms a gray mesh heat-insulating char layer containing $SiO_2$, polycyclic aromatic and $Na_2CO_3$. Meanwhile, the char layer is effective in suppressing the release of toxic and combustible volatiles, such as CO, aliphatic and aromatic compounds. Due to the protection of the exterior regular expanded char layer, more C–C bonds are retained in the interior char layer, which enhance the thermal oxygen resistance and further inhibit the emission of toxic CO. Therefore, introducing Na-Ph-POSS into EP can achieve better catalytic carbonization effect and decrease fire hazards.

### 3.5. Dielectric property

The dielectric constant (ε′) was adopted to measure the ability of charge storage of insulating materials. Besides, dielectric loss (tan δ) refereed to the amount of energy loss due to the degree of dispersion of the substance. With the increase of operating frequency for electronic devices, ideal insulating materials should have low dielectric constant and dielectric loss [40,41]. Digital photos, the dielectric constant curves (a) and dielectric loss curves (b) of EP and its composites just as shown in Fig. 8. Compared to EP, when the addition amount of $T_7$-Ph-POSS was 3 wt%, the dielectric constant and dielectric loss were both reduced slightly. However, increasing the introduced amount of $T_7$-Ph-POSS to 5 wt%, the dielectric constant and dielectric loss were increased significantly. As could been observed in the digital photo of EP/5 wt% $T_7$-Ph-POSS (Fig. 8), a large amount of EP matrix space was remained due to the agglomeration of $T_7$-Ph-POSS. Thus, the dielectric constant and dielectric loss of EP/5 wt% $T_7$-Ph-POSS were similar to that of EP. In contrast, after the introduction of Na-Ph-POSS, the dielectric constant and dielectric loss of EP/Na-Ph-POSS composites were significantly decreased compared to EP, especially for EP/5 wt% Na-Ph-POSS. These results are well related with that with the uniform dispersion of Na-Ph-POSS in EP (just as shown in the digital photo of EP/5 wt% Na-Ph-POSS). Therefore, Na-Ph-POSS has broad application prospects in the electronics field (such as electronic packaging materials and printed circuit boards).

## 4. Conclusions

Sodium-containing polyhedral oligomeric phenyl silsesquioxane (Na-Ph-POSS) was successfully prepared and applied in EP firstly. TG results suggested that Na-Ph-POSS could accelerate the decomposition rate of EP composites and enhance the catalytic carbonization action during the degradation process. The cone calorimeter test results showed that $T_7$-Ph-POSS couldn't promote the formation of an effective protective char layer during combustion. In contrast, Na-Ph-POSS quickly aggregated on the surface of composites during the initial stage of combustion process. Thus, an effective expanded barrier char layer was rapidly formed to prevent the underlying material from further burning. Compared with $T_7$-Ph-POSS, Na-Ph-POSS could distinctly inhibit the volatilization of harmful gases during combustion. It is worth mentioning that the addition of Na-Ph-POSS can significantly decrease the dielectric constant and dielectric loss of composites. Therefore, the successful application of such a metallic POSS in this work provides a new strategy for the design of other metal organic-inorganic hybrid multifunctional flame retardants.

## Declaration of competing interest

The authors declare no conflict of interest.

## CRediT authorship contribution statement

**Xinming Ye:** Writing - original draft, Writing - review & editing. **Jingjing Li:** Methodology, Writing - review & editing. **Wenchao Zhang:** Conceptualization, Supervision, Writing - review & editing. **Rongjie Yang:** Data curation, Funding acquisition, Writing - review & editing. **Jiarong Li:** Supervision, Writing - review & editing.

## Acknowledgements

This project was funded by the National Natural Science Foundation of China (No. 21975022).

## Appendix A. Supplementary data

Supplementary data to this article can be found online at https://doi.org/10.1016/j.compositesb.2020.107961.

## References


[1] Smith RJ, Holder KM, Ruiz S, Hahn W, Song YX, Lvov YM, Grunlan JC. Environmentally benign halloysite nanotube multilayer assembly significantly reduces polyurethane flammability. Adv Funct Mater 2017;28:1703289.

[2] Song PA, Dai JF, Chen GR, Yu YM, Fang ZP, Lei WW, Fu SY, Wang H, Chen ZG. Bioinspired design of strong, tough, and thermally stable polymeric materials via nanoconfinement. ACS Nano 2018;12:9266–78.

[3] Fang F, Ran SY, Fang ZP, Song PA, Wang H. Improved flame resistance and thermo-mechanical properties of epoxy resin nanocomposites from functionalized graphene oxide via self-assembly in water. Compos B Eng 2019;165:406–16.

[4] Li XL, Zhang FH, Jian RK, Ai YF, Ma JL, Hui GJ, Wang DY. Influence of eco-friendly calcium gluconate on the intumescent flame-retardant epoxy resin: flame retardancy, smoke suppression and mechanical properties. Compos B Eng 2019;176:107200.

[5] Huo SQ, Yang S, Wang J, Cheng JW, Zhang QQ, Hu YF, Ding GP, Zhang QX, Song PA. A liquid phosphorus-containing imidazole derivative as flame-retardant curing agent for epoxy resin with enhanced thermal latency, mechanical, and flame-retardant performances. J Hazard Mater 2020;386:121984.

[6] Xu YJ, Shi XH, Lu JH, Qi M, Guo DM, Chen L, Wang YZ. Novel phosphorus-containing imidazolium as hardener for epoxy resin aiming at controllable latent curing behavior and flame retardancy. Compos B Eng 2020;184:107673.

[7] Xiao Y, Jin Z, He L, Ma S, Wang C, Mu X, Song L. Synthesis of a novel graphene conjugated covalent organic framework nanohybrid for enhancing the flame retardancy and mechanical properties of epoxy resins through synergistic effect. Compos B Eng 2020;182:107616.

[8] Zhang QQ, Wang J, Yang S, Cheng JW, Ding GP, Huo SQ. Facile construction of one-component intrinsic flame-retardant epoxy resin system with fast curing ability using imidazole-blocked bismaleimide. Compos B Eng 2019;177:107380.

[9] Mu XW, Wang D, Pan Y, Cai W, Song L, Hu Y. A facile approach to prepare phosphorus and nitrogen containing macromolecular covalent organic nanosheets for enhancing flame retardancy and mechanical property of epoxy resin. Compos B Eng 2019;164:390–9.

[10] Fang F, Song PA, Ran SY, Guo ZH, Wang H, Fang ZP. A facile way to prepare phosphorus-nitrogen-functionalized graphene oxide for enhancing the flame retardancy of epoxy resin. Compos Commun 2018;10:97–102.

[11] Fang F, Huo SQ, Shen HF, Ran SY, Wang H, Song PA, Fang ZP. A bio-based ionic complex with different oxidation states of phosphorus for reducing flammability and smoke release of epoxy resins. Compos Commun 2020;17:104–1108.

[12] Bocio A, Llobet JM, Domingo JL, Corbella J, Teixidó A, Casas C. Polybrominated diphenyl ethers (PBDEs) in foodstuffs: human exposure through the diet. J Agric Food Chem 2003;51:3191–5.

[13] Boer JD. Brominated flame retardants in the environment-the price for our convenience? Environ Chem 2004;1:81–5.

[14] Song GL, Ma SD, Tang GY, Yin ZS, Wang XW. Preparation and characterization of flame retardant form-stable phase change materials composed by EPDM, paraffin and nano magnesium hydroxide. Energy 2010;35:2179–83.

[15] Pang HC, Ning GL, Gong WT, Ye JW, Lin Y. Direct synthesis of hexagonal Mg(OH)2 nanoplates from natural brucite without dissolution procedure. Chem Commun 2011;47:6317–9.

[16] Dasari A, Yu ZZ, Cai GP, Mai YW. Recent developments in the fire retardancy of polymeric materials. Prog Polym Sci 2013;38:1357–87.

[17] Wang X, Kalali EN, Wan JT, Wang DY. Carbon-family materials for flame retardant polymeric materials. Prog Polym Sci 2017;69:22–46.

[18] Yang H, Yu B, Song P, Maluk C, Wang H. Surface-coating engineering for flame retardant flexible polyurethane foams: a critical review. Compos B Eng 2019;176:107185.

[19] Zhang WC, Camino G, Yang RJ. Polymer/polyhedral oligomeric silsesquioxane (POSS) nanocomposites: an overview of fire retardance. Prog Polym Sci 2017;67:77–125.

[20] Wang XX, Zhang WC, Qin ZL, Yang RJ. Optically transparent and flame-retarded polycarbonate nanocomposite based on diphenylphosphine oxide-containing polyhedral oligomeric silsesquioxanes. Compos Appl Sci Manuf 2019;117:92–102.

[21] Ye MF, Wu YW, Zhang WC, Yang RJ. Synthesis of incompletely caged silsesquioxane ($T_7$-POSS) compounds via a versatile three-step approach. Res Chem Intermed 2018;44:4277–94.

[22] Qi Z, Zhang WC, He XD, Yang RJ. High-efficiency flame retardency of epoxy resin composites with perfect $T_8$ caged phosphorus containing polyhedral oligomeric silsesquioxanes (P-POSSs). Compos Sci Technol 2016;127:8–19.

[23] Wu Q, Zhang C, Liang R, Wang B. Combustion and thermal properties of epoxy/phenyltrisilanol polyhedral oligomeric silsesquioxane nanocomposites. J Therm Anal Calorim 2010;100:1009–15.

[24] Ye TP, Liao SF, Zhang Y, Chen MJ, Xiao Y, Liu XY, Liu ZG, Wang DY. Cu(0) and Cu (II) decorated graphene hybrid on improving fireproof efficiency of intumescent flame-retardant epoxy resins. Compos B Eng 2019;175:107189.

[25] Kong Q, Wu T, Zhang J, Wang DY. Simultaneously improving flame retardancy and dynamic mechanical properties of epoxy resin nanocomposites through layered copper phenylphosphate. Compos Sci Technol 2018;154:136–44.

[26] Zhang QR, Li ZW, Li XH, Yu LG, Zhang ZJ, Wu ZS. Zinc ferrite nanoparticle decorated boron nitride nanosheet: preparation, magnetic field arrangement, and flame retardancy. Chem Eng J 2019;356:680–92.

[27] Zhou K, Liu J, Shi Y, Jiang S, Wang D, Hu Y, Gui Z. MoS2 nanolayers grown on carbon nanotubes: an advanced reinforcement for epoxy composites. ACS Appl Mater Interfaces 2015;7:6070–81.

[28] GießMann S, Lorenz V, Liebing P, Hilfert L, Fischer A, Edelmann FT. Synthesis and structural study of new metallasilsesquioxanes of potassium and uranium. Dalton Trans 2017;46:2415–9.

[29] Denise P, Christian L. Iron silicates, iron-modulated zeolite catalysts, and molecular models thereof. Chem Eur J 2014;20:9166–75.

[30] Wu HY, Zeng BR, Chen JM, Wu T, Li YT, Liu YZ, Dai LZ. An intramolecular hybrid of metal polyhedral oligomeric silsesquioxanes with special titanium-embedded cage structure and flame retardant functionality. Chem Eng J 2019;374:1304–16.

[31] Dronova MS, Bilyachenko AN, Yalymov AI, Kozlov YN, Shul'Pina LS, Korlyukov AA, Arkhipov DE, Levitsky MM, Shubina ES, Shul'Pin GB. Solvent-controlled synthesis of tetranuclear cage-like copper (ii) silsesquioxanes. Remarkable features of the cage structures and their high catalytic activity in oxidation with peroxides. Dalton Trans 2013;43:872–82.

[32] Krug DJ, Laine RM. Durable and hydrophobic organic-inorganic hybrid coatings via fluoride rearrangement of phenyl $T_{12}$ silsesquioxane and siloxanes. ACS Appl Mater Interfaces 2017;9:8378–83.

[33] Kalali EN, Wang X, Wang DY. Multifunctional intercalation in layered double hydroxide: toward multifunctional nanohybrid for epoxy resin. J Mater Chem 2016;4:2147–57.

[34] Guo W, Nie S, Kalali EN, Wang X, Wang W, Cai W, Song L, Hu Y. Construction of $SiO_2$@UiO-66 core-shell microarchitectures through covalent linkage as flame retardant and smoke suppressant for epoxy resins. Compos B Eng 2019;176:107261.

[35] Li XW, Feng YZ, Chen C, Ye YS, Zeng HX, Qu H, Liu JW, Zhou XP, Long SJ, Xie XL. Highly thermally conductive flame retardant epoxy nanocomposites with multifunctional ionic liquid flame retardant-functionalized boron nitride nanosheets. J Mater Chem 2018;6:20500–12.

[36] Li XS, Zhao ZL, Wang YH, Yan H, Zhang XY, Xu BS. Highly efficient flame retardant, flexible, and strong adhesive intumescent coating on polypropylene using hyperbranched polyamide. Chem Eng J 2017;324:237–50.

[37] Yuan GW, Yang B, Chen YH, Jia YG. Synthesis of a novel multi-structure synergistic POSS-GO-DOPO ternary graft flame retardant and its application in polypropylene. Compos Appl Sci Manuf 2019;117:345–56.

[38] Zhang WC, Li XM, Fan HB, Yang RJ. Study on mechanism of phosphorus-silicon synergistic flame retardancy on epoxy resins. Polym Degrad Stabil 2012;97:2241–8.

[39] Xu WZ, Zhang BL, Wang XL, Wang GS, Ding D. The flame retardancy and smoke suppression effect of a hybrid containing CuMoO4 modified reduced graphene oxide/layered double hydroxide on epoxy resin. J Hazard Mater 2018;343:364–75.

[40] Jiao YC, Yuan L, Liang GZ, Gu AJ. Dispersing carbon nanotubes in the unfavorable phase of an immiscible reverse-phase blend with Haake instrument to fabricate high-k nanocomposites with extremely low dielectric loss and percolation threshold. Chem Eng J 2016;285:650–9.

[41] Xu YJ, Chen L, Rao WH, Qi M, Guo DM, Liao W, Wang YZ. Latent curing epoxy system with excellent thermal stability, flame retardance and dielectric property. Chem Eng J 2018;347:223–32.